# Enhanced optical nonlinearity of Mxene Ti<sub>3</sub>C<sub>2</sub>T<sub>x</sub> nanosheets decorated with silver nanoparticles

LIHE YAN, D YANMIN XU, JINHAI SI, YUREN LI, AND XUN HOU

Key Laboratory for Physical Electronics and Devices of the Ministry of Education & Shaanxi Key Lab of Photonic Technique for information, School of Electronics science & Engineering, Faculty of Electronic and Information Engineering, Xi'an Jiaotong University, Xi'an, 710049, China  $^st$ jinhaisi@mail.xjtu.edu.cn

**Abstract:** Two-dimensional  $Ti_3C_2T_x$  nanosheets have drawn much attention due to their unique nonlinear optical properties. To enhance the optical nonlinearity of the material, we synthesized  $Ti_3C_2T_x$  composites decorated with silver nanoparticles ( $Ti_3C_2T_x/Ag$ ) through self-assembling of Ag nanoparticles on the surface of  $Ti_3C_2T_x$ . The nonlinear optical properties the composite were studied via nanosecond laser Z-scan method, and enhanced saturable absorption (SA) and reversed saturable absorption (RSA) effects were demonstrated. Using the femtosecond time-resolved transient absorption measurements, the carrier dynamics in the nonlinear response, as well as the enhancement mechanism of the composites was clarified.

© 2021 Optical Society of America under the terms of the OSA Open Access Publishing Agreement

#### Introduction

Nonlinear optical materials, with strong electrical conductivity, large tunable bandwidth, thermally stability, and so on, have attracted much attention due to their extensive applications in laser mode locking, optical limiting, and lasing [1–4]. In the past few decades, different kinds of nonlinear materials like semiconductors, organic molecules, inorganic glasses and crystals, and nanomaterials have been widely studied [5–8]. Developing new materials with strong optical nonlinear properties and ultrafast response time have always been the research hotspot. Recently, two-dimensional (2D) materials like graphene, transition metal sulfides nanosheets have also attracted remarkable research interests due to their good nonlinear optical properties [9–11]. As a newly emerged 2D material, MXene materials have aroused extraordinary attention in optical, energy storage, catalysis fields, attributing to their high conductivities, tunable band gap and so on [12–14]. Typically, MXene is fabricated from transition-metal carbide, nitrides, or carbonitrides with MAX phase, where M and A are the transition metal and main group elements, and X represents C or N elements. By etching the A-layer with HF or HCl/LiF solution, the lamellar accordion structure of MXene can be obtained [15,16]. Among the MXene materials,  $T_{i_3}C_2T_x$  is the most widely reported since it was firstly discovered in 2011 [17]. Due to the acid environment, abundant active functional groups ( $T_x=-0$ , -OH and/or -F) are linked to the  $Ti_3C_2T_x$  surface during the process, which not only provide well hydrophilic property, but also make  $T_{i_3}C_2T_x$ have good electrical conductivity [18,19].

The unique chemical and physical properties make  $Ti_3C_2T_x$  idea material for super-supercapacitors, lithium batteries, energy storage, microwave absorption and so on [20-22]. In the optical area, Ti<sub>3</sub>C<sub>2</sub>T<sub>x</sub> shows great nonlinear optical performance and has gained extensively attention in recent years [17,23]. For example, Miao et al investigated the nonlinear optical response of  $Ti_3C_2T_x$  via spatial self-phase modulation (SSPM), and found that  $Ti_3C_2T_x$  exhibited broadband nonlinear optical response from 400 nm to ~1 µm [24]. Jiang's group studied the nonlinear optical property of Ti<sub>3</sub>C<sub>2</sub>T<sub>x</sub> over near-infrared area (800-1800nm), which showed a giant nonlinear absorption coefficient of  $10^{-13}$  esu [14] [19,25]. Moreover, some Ti<sub>3</sub>C<sub>2</sub>T<sub>x</sub> composites have been proposed to extend their applications in different areas, and interesting results in the optical filed have been reported. Xie et al designed  $Ti_3C_2T_x$  and gold nanorods

https://doi.org/10.1364/OME.422189 Received 8 Feb 2021; revised 19 Mar 2021; accepted 22 Mar 2021; published 9 Apr 2021

(AuNRs) composite by electrostatic self-assembly method [16], realizing the effectively detection of organic pollutants through the Surface-Enhanced Raman Scattering (SERS) effect. Yue's group synthesized  $Ti_3C_2T_x$ /Au nanocomposite using  $Ti_3C_2T_x$  and HAuCl<sub>4</sub> as the reagents, which showed a strong SERS effect [26]. Although the  $Ti_3C_2T_x$  composites have been well prepared and applied in various fields successfully, the nonlinear optical characteristic, especially the carrier dynamics have rarely been reported.

Herein, we synthesize  $T_{i_3}C_2T_x$  composites decorated with silver nanoparticles  $(T_{i_3}C_2T_x/Ag)$  by reducing Ag ions in  $T_{i_3}C_2T_x$  aqueous solution based on the strong reducing property of the surface functional groups on the nanosheets. The physical and chemical structures of the material are characterized using a transmission electron microscope (TEM), scanning electron microscope (SEM), X-ray diffraction (XRD), X-ray photoelectron spectroscopy (XPS) and UV-Vis absorption spectroscopy. The enhanced nonlinear saturable absorption (SA) and reversed saturable absorption (RSA) effects of  $T_{i_3}C_2T_x/Ag$  composite are observed by nanosecond laser Z-scan method. Using the femtosecond time-resolved transient absorption (TA) measurements, carrier dynamics and enhancement mechanism of the nonlinear response are clarified.

#### 2. Materials and methods

#### 2.1. Materials

The monolayer  $Ti_3C_2T_x$  nanosheets and dispersant containing nonionic surfactant with aromatic groups are purchased from Jiangsu XFNANO Materials Tech Co., Ltd. (Nanjing, China). The silver nitrate (AgNO<sub>3</sub>, 99.8% wt. %, purity) is obtained from Sinopharm Chemical Reagent Co., Ltd (Beijing, China). The deionized water is used throughout the experiment to prepare the samples. All chemicals used in this experiment are without further purification.

### 2.2. Synthesis of the $Ti_3C_2T_x/Ag$ composite

The  $Ti_3C_2T_x/Ag$  composite are prepared by mixing the  $Ti_3C_2T_x$  nanosheets dispersion and  $AgNO_3$  solution. First, 1 mL of  $Ti_3C_2T_x$  dispersion (2.5 mg/mL) is dispersed in 7 mL deionized water mixed with 1 mL of dispersant. Then, the dispersion is sonicated in an ultrasonic bath continuously for 30 minutes. Next, 400  $\mu$ L of  $AgNO_3$  solution (5 mg/mL) is added into the above dispersion, continuing to sonicate for 25 minutes. Finally, dark green dispersion containing  $Ti_3C_2T_x/Ag$  composite is obtained.

#### 2.3. Instruments and measurements

The TEM images and high-resolution TEM (HRTEM) images of the  $Ti_3C_2T_x/Ag$  composite are obtained using a JEM-ARM200F high-resolution transmission electron microscope (Japan). SEM (SU3500, China) is used to acquire the morphologies of the synthesized composite. XRD patterns are measured using an X-ray diffractometer (X'PERT PRO PANALYTICAL, Netherlands), and XPS experiments are performed on an X-ray photoelectron spectrometer (ESCALAB Xi<sup>+</sup>, USA). A UV-Vis spectrophotometer (UV-2600, China).is used for measuring the absorption spectra of samples. The atomic force microscopy (AFM) image is obtained using an atomic force microscope (RENISHAW, UK).

A nanosecond open aperture Z-scan setup is employed to study the nonlinear absorption property of  $Ti_3C_2T_x/Ag$  composite. A nanosecond pulse laser centered at 532 nm with pulse width of 10 ns and repetition rate of 10 Hz is used as the light source. The laser pulses are focused using an f=20 cm lens and then injected onto the samples. The samples are filled in a 1 mm thick quartz cells, and the linear transmittance of all samples is adjusted to be 60%. The samples are fixed on a translation stage moving along the Z-axis direction, and a pulse energy meter is used to record the transmittance change as a function of the distance between the materials and the laser focus.

The photoinduced carrier dynamics in the nonlinear absorption process of  $Ti_3C_2T_x/Ag$  composite is detected using a homebuilt femtosecond time-resolved TA system. In the experiment, a Ti: sapphire mode-locked laser centered at 800 nm with pulse width of 100fs and repetition rate of 1 kHz, is used as the light source. The laser beam is spitted into two parts: the stronger one is frequency doubled using a BBO crystal generating a 400 nm pump light; the weaker one is focused into a sapphire plate to generate a broadband supercontinuum used as the probe light. The pump and probe beams are focused and overlapped in the samples. The pump pulses are used to excite the samples and the probe pluses are used to detect the absorption change of the samples. By controlling the arriving time at the sample of pump and probe lights, the optical density changes are recorded by a fiber spectroscopy.

#### 3. Results and discussions

#### 3.1. Materials and characterizations

The morphologic structures of the composite are characterized by the TEM and HRTEM images. Figure 1(a) shows that  $Ti_3C_2T_x$  nanosheets flat on the substrate, and Ag nanoparticles with tens of nanometers are deposited on the  $Ti_3C_2T_x$  surface. Figure 1(b) presents the size distribution of the Ag nanoparticles mainly in the range of 20-50 nm with a mean size of 32 nm. The lattice spacing shown in HRTEM image (Fig. 1(c)) is 0.238 nm (marked in the blue block), corresponding to the Ag (111) crystal plane [21]. The HRTEM image with red border shows the clear lattice fringes (0.27 nm), which are associated with the (0110) plane of the  $Ti_3C_2$  phase [16]. The AFM image and the height profile of  $Ti_3C_2T_x$  nanosheet (Fig. 1(d)) exhibit typical topographic heights less than 1 nm, indicating the monolayer property of  $Ti_3C_2T_x$  [14]. The SEM image in Fig. 1(e) indicates the Ag nanoparticles (the bright particles) are decorated on the surface of the  $Ti_3C_2T_x$  densely [27]. Figure 1(f) displays photographs of  $Ti_3C_2T_x$  and  $Ti_3C_2T_x/Ag$  composite dispersions. The color of the samples changes from black to dark green when Ag nanoparticles are decorated on  $Ti_3C_2T_x$ . XRD measurement is used to study the phase structures of  $Ti_3C_2T_x$  and  $Ti_3C_2T_x/Ag$  composite. The XRD pattern (Fig. 1(g)) of  $Ti_3C_2T_x/Ag$  composite shows four peaks at 38.2°, 44.2°, 64.3°, and 77.7°, corresponding to the (111), (200), (220), and (311) planes

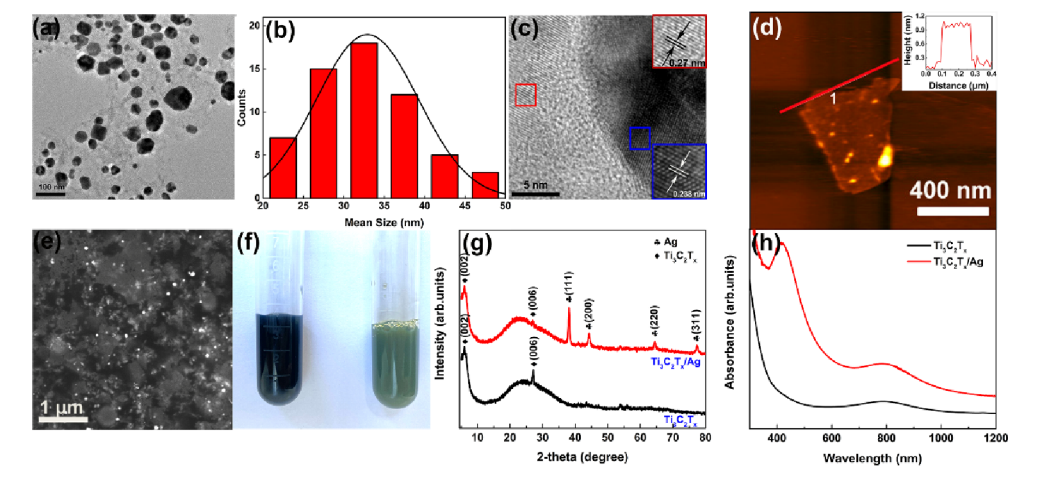


**Fig. 1.** (a) TEM image of  $Ti_3C_2T_x/Ag$  composite. (b) The size distribution of Ag nanoparticles. (c) HRTEM image of the composite. (d) AFM images of the  $Ti_3C_2T_x$  (the inset is the height of nanosheets). (e) SEM image of the composite. (f) Photographs of  $Ti_3C_2T_x$  (left) and  $Ti_3C_2T_x/Ag$  composite (right). (g) XRD patterns, and (h) UV-Vis absorption spectra of  $Ti_3C_2T_x$  and  $Ti_3C_2T_x/Ag$  composite.

of the Ag single crystals [28,29], respectively. The two peaks at  $6^{\circ}$  and  $28^{\circ}$  are corresponding to the (002) and (006) plans of  $Ti_3C_2$ , as the same as pure  $Ti_3C_2T_x$  (the black line). The absorption spectrum of the pure  $Ti_3C_2T_x$  in Fig. 1(h) shows a broadband absorption ranging from the visible to near-infrared range [24]. The  $Ti_3C_2T_x/Ag$  composite exhibits a strong absorption peak at  $\sim$ 430 nm, attributing to the formation of Ag nanoparticles [30,31]. All the above data prove that the  $Ti_3C_2T_x/Ag$  composite is synthesized successfully.

XPS is performed to characterize the chemical structure of the samples. Figure 2(a) displays that Ti, C, O and F elements can be detected in both materials.  $C1_s$  and  $O1_s$  peaks in the samples demonstrate that the surfaces of  $Ti_3C_2T_x$  are functionalized by OH groups [32], and Ag 3d peak (367 eV) is observed in the composite. Figure 2(b) and (c) shows the high resolution spectra of Ti 2p in both materials. The peak at 458.8 eV from original samples is assigned to Ti (IV) 2p3/2 [31], and the peaks at 455 and 456.9 eV belong to Ti (II) 2p3/2 and Ti (III) 2p3/2, respectively [29]. The broad peaks ranging from 461-465 eV in Fig. 2(b) suggests the possible presence of high valence Ti species (Ti-C (461.5 eV) and Ti (IV) (464.3 eV)) [27]. After decorated with Ag nanoparticles, the locations of Ti (II), Ti (III) and Ti (IV) species have a shift and the Ti (IV) peak disappears, which might derive from the formation of metallic Ag [28]. Figure 2(d) reveals the high resolution spectra of Ag 3d in the composite. The XPS spectra of Ag 3d can be fitted two bands: Ag 3d5/2 (366.8 eV) and Ag 3d3/2 (372.8 eV), indicating that only the metallic Ag is formed in the nanoparticles, and other states of the Ag are negligible [32].

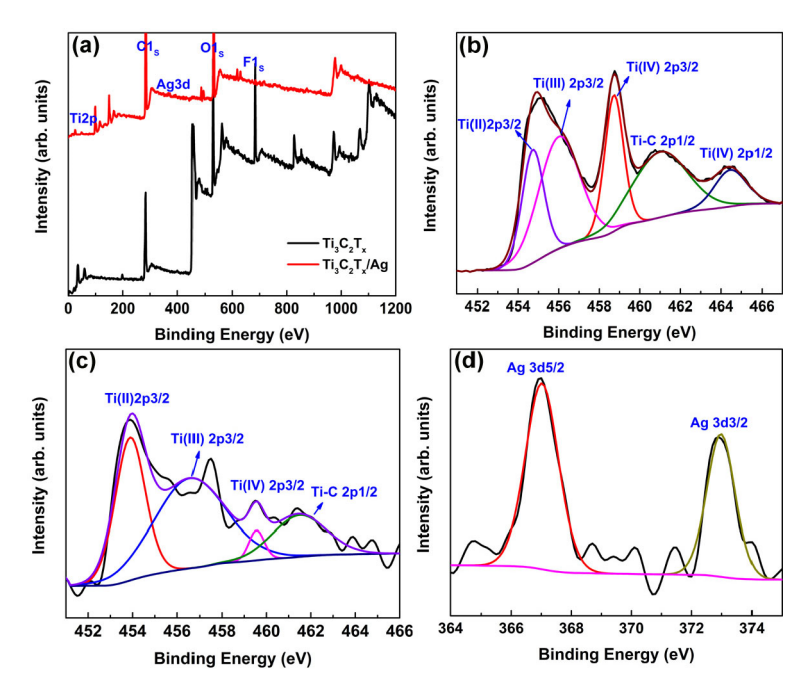


**Fig. 2.** (a) XPS patterns of  $Ti_3C_2T_x$  and  $Ti_3C_2T_x/Ag$  composite. (b) High-resolution XPS spectra for  $Ti_3C_2T_x$ . (c)  $Ti_3C_2T_x$  and (d)  $Ag_3d_3$  high-resolution XPS spectra of  $Ti_3C_2T_x/Ag$  composite.

#### 3.2. Nonlinear optical properties

The Z-can measurement is carried out to investigate the optical nonlinearity of  $Ti_3C_2T_x/Ag$  composite. The laser pulses from a nanosecond laser (central wavelength: 532 nm) is focused by a lens (focus length: 200 mm), and then injected into the samples. The nonlinear transmittance changes are recorded through adjusting the distance between samples and the beam focus.

Figure 3(a) shows the optical nonlinearity of the  $Ti_3C_2T_x$  nanosheets and  $Ti_3C_2T_x/Ag$  composite under the same laser pulse energy. With the sample moving to the focus, the pulse energy density increases, and the transmittance of the samples both increase firstly and then decrease near the focus. The Z-scan profiles of the samples consist of three different parts: (1) linear absorption far from the focus, (2) SA effect near the focus, and (3) RSA behavior around the focus [33]. From the results we can see that, the  $Ti_3C_2T_x/Ag$  composite have stronger SA and RSA effects compared with that of the pure  $Ti_3C_2T_x$ , indicating an enhanced interaction between Ag nanoparticles and  $Ti_3C_2T_x$  nanosheets. Figure 3(b) shows the Z-scans curves under various incident power intensity values for  $Ti_3C_2T_x/Ag$  composite. When the incident pulse energy increases, the nonlinear transmittance of the  $Ti_3C_2T_x/Ag$  composite decreases correspondingly, demonstrating a stronger RSA behavior.

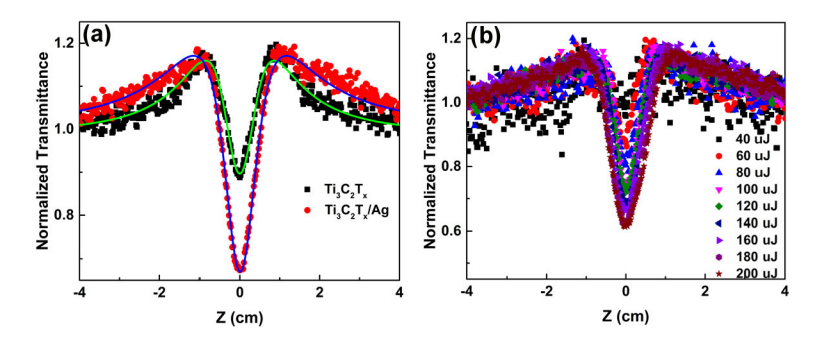


**Fig. 3.** (a) Z-scan results for  $Ti_3C_2T_x$  and  $Ti_3C_2T_x/Ag$  composite at 532 nm. (b) Z-scans curves under various laser intensity values for  $Ti_3C_2T_x/Ag$  composite.

In Z-scan measurements, the following equation is used to fit the nonlinear absorption coefficients, including saturable intensity Is and the RSA coefficient  $\beta$ :

$$T(z) = \exp(-(\alpha_0/(1 + I(z)/I_s) + \beta I(z))l_0)$$

Where  $\alpha_0$  stands for the linear absorption coefficient, and  $l_0$  is the optical path in the sample. I(z) is the laser intensity at different positions along Z direction, and can be expressed as  $I(z) = I/\pi\omega(z)^2$ , in which the Gaussian beam radius  $\omega(z) = \omega_0(1+z^2/z_R^2)$ , and  $Z_R$  is the Rayleigh length of the Gaussian beam [34,35]. By fitting the Z-scan profiles of the samples, the values of  $I_s$  and  $\beta$  of samples are obtained and summarized in Table 1. The nonlinear coefficients of pure  $Ti_3C_2T_x$  agree well with the values given in the previous reports [36–38]. Compared with the pure  $Ti_3C_2T_x$ , the  $I_s$  of the  $Ti_3C_2T_x/Ag$  composite is lower by almost 1 order, and the  $\beta$  value is enhanced by near 3 times. In the composite, Ag nanoparticles could contribute the nonlinear absorption effect. In some previous reports, the nonlinear response of pure Ag nanoparticles has been observed when the material was irradiated by light with intensity of ~10 GW/cm<sup>2</sup> [33]. This value is much higher than that used in our experiments, which was estimated to be in the order of ~100 MW/cm<sup>2</sup>. Therefore, the contribution of Ag nanoparticles to the nonlinear optical property of the composite can be ruled out, and the interactions between  $Ti_3C_2T_x$  and Ag nanoparticles may cause the enhanced nonlinear response in the  $Ti_3C_2T_x/Ag$  composite.

Table 1. NLO coefficients of Ti<sub>3</sub>C<sub>2</sub>T<sub>x</sub>/Ag composite and Ti<sub>3</sub>C<sub>2</sub>T<sub>x</sub> fitting from the experimental data analysis in Fig. 3.

Samples	I <sub>s</sub> (MW/cm <sup>2</sup> )	$\beta$ (cm MW <sup>-1</sup> )	
$Ti_3C_2T_x$	109.50857	0.08587	
Ti <sub>3</sub> C <sub>2</sub> T <sub>x</sub> /Ag composite	13.36257	0.28284	

The mechanism and carrier dynamics in the nonlinear optical response of  $Ti_3C_2T_x/Ag$  composite are studied using a femtosecond time-resolved TA spectroscopy. The corresponding TA spectra of both samples are shown in Fig. 4. Both the samples are excited under the same pump intensity. The TA spectra of  $Ti_3C_2T_x$  (Fig. 4(a)) exhibits a broad positive signal in the range of 450 to 700 nm, indicating that excited state absorption dominates after the sample is excited [24]. The weak and irregular negative signals in the TA spectra are mainly originated from the noises in the measurement. When  $Ti_3C_2T_x$  is excited by laser, electrons in the valence band (VB) could be excited to the conduction band (CB). This process would cause bleaching effect in VB, which could suppress the absorption of the incident light, inducing the SA effect. Before the excited electrons decay back to the VB, they could further transfer to the surface functional groups, causing a strong absorption on the surface states. This surface states absorption will cause an RSA effect in the Z-scan measurements.

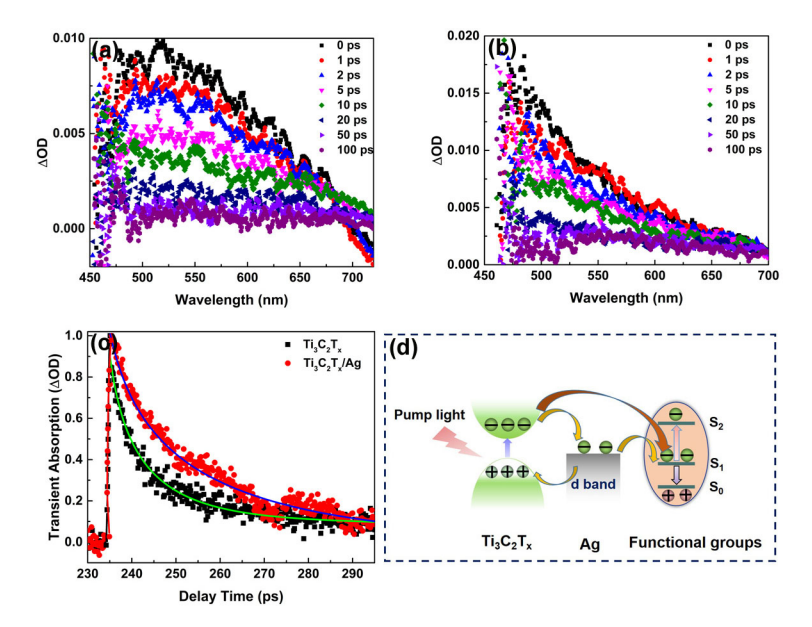


**Fig. 4.** Femtosecond TA spectra of (a)  $Ti_3C_2T_x$  and (b)  $Ti_3C_2T_x/Ag$  composite probed at different delay times under 400 nm excitation. (c) Carrier dynamics of  $Ti_3C_2T_x$  and  $Ti_3C_2T_x/Ag$  composite under the same laser intensity. (d) Diagram of the charge-transfer process in  $Ti_3C_2T_x/Ag$  composite.

When decorated by Ag nanoparticles, electrons transfer between  $Ti_3C_2T_x$  and Ag atoms could take place. Figure 4(b) describes the TA spectra of the  $Ti_3C_2T_x/Ag$  composite, and the excited state absorption can be observed. The enhanced absorption (compared with pure  $Ti_3C_2T_x$ ) at short wavelength may be due to absorption of photo-induced surface plasmon in Ag nanoparticles [39]. Figure 4(c) summarizes the decay process of absorption change at 520 nm in  $Ti_3C_2T_x$  and  $Ti_3C_2T_x/Ag$  composite. The decay processes of samples are fitted using multi-exponential decay function, and the corresponding nonlinear coefficients are listed in Table 2. The  $Ti_3C_2T_x$  shows two relaxation processes: a fast relaxation time (5 ps) corresponds to the cooling of hot carriers and the recombination time of the electrons-holes [24]; a slow relaxation time (39 ps) attributed to the relaxation of carriers from  $Ti_3C_2T_x$  to the surface functional groups [40]. Similar with the pure  $Ti_3C_2T_x$ , the carrier dynamic process of  $Ti_3C_2T_x/Ag$  composite also consist of a fast and a slow relaxation time, while the proportion of slow process has increased (from 42% to 58%). To illustrate the carrier dynamics process of the  $Ti_3C_2T_x/Ag$  composite, a schematic diagram is proposed in Fig. 4(d). Due to Ag has large states density, the excited electrons in

#### 1407

## Optical Materials EXPRESS

the CB of  $Ti_3C_2T_x$  would like to transfer to the d band of Ag atoms before the bleaching effect of VB vanishes [33]. This process will prolong the lifetime of excited electrons in composite, causing the stronger SA response. Besides, the electrons in the d band of Ag atoms would further transfer to the excited state of the functional groups, which will absorb the incident light and jump to the higher energy level, inducing the enhanced RSA performance. In summary, the TA results revealed that, the enhanced nonlinear optical behavior in  $Ti_3C_2T_x/Ag$  composite could be attributed to the strong interaction between  $Ti_3C_2T_x$  and Ag nanoparticles.

Table 2. Fitted coefficients for TA curves in Fig. 4 using a double exponential decay function of  $A_1 \times e^{t/\tau_1} + A_2 \times e^{t/\tau_2}$ .

Samples	τ <sub>1</sub> (ps)	$A_1$	τ <sub>2</sub> (ps)	A <sub>2</sub>
Ti <sub>3</sub> C <sub>2</sub> T <sub>x</sub>	5	66%	39	34%
Ti <sub>3</sub> C <sub>2</sub> T <sub>x</sub> /Ag composite	6	42%	35	58%

#### 4. Conclusion

In summary, we synthesized  $Ti_3C_2T_x/Ag$  composite by reducing Ag ions in  $Ti_3C_2T_x$  aqueous solution, and Ag nanoparticles were decorated on the  $Ti_3C_2T_x$  nanosheets uniformly. The nonlinear optical properties of the composite were studied using nanosecond open-aperture Z-scan and femtosecond time-resolved TA techniques. The results indicated that, ground state bleaching occurred under intense light irradiation in pure  $Ti_3C_2T_x$ , inducing a strong SA effect, and excited state absorption of the surface functional groups caused the RSA response. When decorated with Ag nanoparticles, excited electrons trended to transfer from  $Ti_3C_2T_x$  to Ag, prolonging the carrier relaxation time of the composites and leading to the stronger SA effect. Besides, the carriers on the d band of Ag would further transfer to the excited state of the functional groups, and the induced exited states absorption resulted in the enhanced RSA response in the  $Ti_3C_2T_x/Ag$  composite.

**Funding.** the National R&D Program of China (2019YFA0706402); National Natural Science Foundation of China (62027822); National Natural Science Foundation of China (61690221); the Key research and Development Program of Shaanxi province (2017ZDXM-GY-120).

**Acknowledgements.** This work was supported by the National R&D Program of China (2019YFA0706402); National Natural Science Foundation of China (62027822 and 61690221); the Key research and Development Program of Shaanxi province (2017ZDXM-GY-120).

**Disclosures.** The authors declare no conflicts of interest.

#### References

- L. H. Yan, X. F. Wang, J. H. Si, S. Matsuo, T. Chen, W. J. Tan, F. Chen, and X. Hou, "Time-resolved single-shot imaging of femtosecond laser induced filaments using supercontinuum and optical polarigraphy," Appl. Phys. Lett. 100(11), 111107 (2012).
- X. L. Sun, B. T. Zhang, Y. L. Li, X. Y. Luo, G. R. Li, Y. X. Chen, C. Q. Zhang, and J. L. He, "Tunable ultrafast nonlinear optical properties of graphene/MoS<sub>2</sub> van der Waals heterostructures and their application in solid-state bulk lasers," ACS Nano 12(11), 11376–11385 (2018).
- Y. Yu, L. H. Yan, M. M. Yue, and H. H. Xu, "Femtosecond laser-assisted synthesis of silver nanoparticles and reduced graphene oxide hybrid for optical limiting," R. Soc. Open Sci. 5(7), 171436 (2018).
- C. J. Quan, C. H. Lu, C. He, X. Xu, Y. Y. Huang, Q. Y. Zhao, and X. L. Xu, "Band alignment of MoTe<sub>2</sub>/MoS<sub>2</sub> nanocomposite films for enhanced nonlinear optical performance," Adv. Mater. Interfaces 6(5), 1801733 (2019).
- S. B. Bettis, V. K. Sangwan, I. Balla, H. Bergeron, E. A. Weiss, and M. C. Hersam, "Ultrafast exciton dissociation and long-lived charge separation in a photovoltaic Pentacene-MoS<sub>2</sub> van der Waals heterojunction," Nano Lett. 17(1), 164–169 (2017).
- G. J. Ye, T. T. Zhao, Z. N. Jin, P. Y. Gu, J. Y. Mao, Q. H. Xu, Q. F. Xu, J. M. Lu, N. J. Li, and Y. L. Song, "The synthesis and NLO properties of 1,8-naphthalimide derivatives for both femtosecond and nanosecond laser pulses," Dyes Pigments 94(2), 271–277 (2012).
- O. M. Pearce, J. S. Duncan, N. H. Damrauer, and G. Dukovic, "Ultrafast hole transfer from CdS quantum dots to a water oxidation catalyst," J. Phys. Chem. C 122(30), 17559–17565 (2018).

- 8. Q. Tong, Y. H. Wang, X. X. Yu, B. Wang, Z. Liang, M. Tang, A. S. Wu, H. J. Zhang, F. Liang, Y. F. Xie, and J. Wang, "Nonlinear optical and multi-photon absorption properties in graphene-ZnO nanocomposites," Nanotechnology **29**(16), 165706 (2018).
- 9. L. Wang, Z. Wang, H. Y. Wang, H. Y. Wang, G. Grinblat, Y. L. Huang, D. Wang, X. H. Ye, X. B. Li, Q. L. Bao, A. T. S. Wee, S. A. Maier, Q. D. Chen, M. L. Zhong, C. W. Qiu, and H. B. Sun, "Slow cooling and efficient extraction of C-exciton hot carriers in MoS<sub>2</sub> monolayer," Nat. Commun. 8(1), 13906 (2017).
- 10. G. Z. Wang, K. P. Wang, B. M. Szydłowska, A. A. B. Murray, J. J. Wang, Y. Y. Feng, X. Y. Zhang, J. Wang, and W. J. Blau, "Ultrafast nonlinear optical properties of a graphene saturable mirror in the 2 µm wavelength region," Laser Photonics Rev. 11(5), 1700166 (2017).
- 11. W. J. Liu, M. L. Liu, B. Liu, R. G. Quhe, M. Lei, S. B. Fang, H. Teng, and Z. Y. Wei, "Nonlinear optical properties of MoS<sub>2</sub>-WS<sub>2</sub> heterostructure in fiber lasers," Opt. Express 27(5), 6689 (2019).
- 12. T. C. Jiang, Y. S. Huang, and X. Q. Meng, "CdS core-Au/MXene-based photodetectors: Positive deep-UV photoresponse and negative UV-Vis-NIR photoresponse," Appl. Surf. Sci. 513, 145813 (2020).
- 13. Y. Cao, Q. H. Deng, Z. D. Liu, D. Y. Shen, T. Wang, Q. Huang, S. Y. Du, N. Jiang, C. T. Lin, and J. H. Yu, "Enhanced thermal properties of poly (vinylidene fluoride) composites with ultrathin nanosheets of MXene," RSC Adv. 7(33), 20494-20501 (2017).
- 14. A. Zhang, R. Liu, J. M. Tian, W. G. Huang, and J. Q. Liu, "MXene-based nanocomposites for energy conversion and storage applications," Chem. Eur. J. 26(29), 6342–6359 (2020).
- 15. D.D. Song, X.Y. Jiang, Y.S. Li, X. Lu, S. R. Luan, Y. Z. Wang, Y. Li, and F. Gao, "Metal-organic frameworks-derived  $MnO_2/Mn_3O_4$  microcuboids with hierarchically ordered nanosheets and  $Ti_3C_2$  MXene/Au NPs composites for electrochemical pesticide detection," J. Hazard. Mater. 373, 367-376 (2019).
- 16. H. H. Xie, P. H. Li, J. D. Shao, H. Huang, Y. Chen, Z. Y. Jiang, P. K. Chu, and X. F. Yu, "Electrostatic self-assembly of Ti<sub>3</sub>C<sub>2</sub>T<sub>x</sub> MXene and gold nanorods as an efficient Surface-Enhanced Raman Scattering platform for reliable and high-sensitivity determination of organic pollutants," ACS Sens. 4(9), 2303–2310 (2019).
- 17. T. C. Feng, X. H. Li, P. L. Guo, Y. Zhang, J. S. Liu, and H. Zhang, "MXene: two dimensional inorganic compounds, for generation of bound state soliton pulses in nonlinear optical system," Nanophotonics 9(8), 2505–2513 (2020).
- 18. Z. H. Zhou, W. Panatdasirisuk, T. S. Mathis, B. Anasori, C. Lu, X. X. Zhang, Z. W. Liao, Y. Gogotsi, and S. Yang, "Layer-by-layer assembly of MXene and carbon nanotubes on electrospun polymer films for flexible energy storage," Nanoscale **10**(13), 6005–6013 (2018).
- 19. X. T. Jiang, S. X. Liu, W. Y. Liang, S. J. Luo, Z. L. He, Y. Q. Ge, H. D. Wang, R. Cao, F. Zhang, Q. Wen, J. Q. Li, Q. L. Bao, D. Y. Fan, and H. Zhang, "Broadband nonlinear photonics in few-layer MXene Ti<sub>3</sub>C<sub>2</sub>T<sub>x</sub> (T = F, O, or OH)," Laser Photonics Rev. 12(2), 1700229 (2018).
- 20. K. K. Li, T. F. Jiao, R. R. Xing, G. D. Zou, J. X. Zhou, L. X. Zhang, and Q. M. Peng, "Fabrication of tunable hierarchical MXene@AuNPs nanocomposites constructed by self-reduction reactions with enhanced catalytic performances," Sci. China Mater. 61(5), 728-736 (2018).
- 21. X. X. Huang, R. Wang, T. F. Jiao, G. D. Zou, F. K. Zhan, J. J. Yin, L. X. Zhang, J. X. Zhou, and Q. M. Peng, "Facile preparation of hierarchical Ag NP-loaded MXene/Fe<sub>3</sub>O<sub>4</sub>/polymer nanocomposites by electrospinning with enhanced catalytic performance for wastewater treatment," ACS Omega 4(1), 1897-1906 (2019).
- 22. J. J. Fu, L. Li, J. M. Yun, D. Lee, B. K. Ryu, and K. H. Kima, "Two-dimensional titanium carbide (MXene)-wrapped sisal-Like NiCo<sub>2</sub>S<sub>4</sub> as positive electrode for High-performance hybrid pouch-type asymmetric supercapacitor," Chem. Eng. J 375, 121939 (2019).
- 23. Y. C. Dong, S. Chertopalov, K. Maleski, B. Anasori, L. Y. Hu, S. Bhattacharya, A. M. Rao, Y. Gogotsi, V. N. Mochalin, and R. Podila, "Saturable absorption in 2D Ti<sub>3</sub>C<sub>2</sub> MXene thin films for passive photonic diodes," Adv. Mater. **30**(10), 1705714 (2018).
- 24. J. Li, Z. L. Zhang, J. Yi, L. L. Miao, J. Huang, J. R. Zhang, Y. He, B. Huang, C. J. Zhao, Y. H. Zou, and S. C. Wen, "Broadband spatial self-phase modulation and ultrafast response of MXene  $Ti_3C_2T_x$  (T = O, OH or F)," Nanophotonics 9(8), 2415–2424 (2020).
- 25. X. Y. Chen, Y. Y. Zhao, L. Z. Li, Y. H. Wang, J. L. Wang, J. J. Xiong, S. L. Du, P. Zhang, X. R. Shi, and J. H. Yu, "MXene/polymer nanocomposites: preparation, properties, and applications," Poly. Rev. 61(1), 80–115 (2021).
- 26. M. Yue, F. Li, N. H. Lu, P. Yao, T. Xue, and P. Liu, "Synthesis of two-dimensional Ti<sub>3</sub>C<sub>2</sub>T<sub>x</sub>/Au nanosheets with SERS performance," Appl. Opt. **58**(30), 8290–8294 (2019).
- 27. C. Ji, Y. Wang, Z. Q. Ye, L. Y. Tan, D. S. Mao, W. G. Zhao, X. L. Zeng, C. Z. Yan, R. Sun, D. J. Kang, J. B. Xu, and C. P. Wong, "Ice-templated MXene/Ag-epoxy nanocomposites as high-performance thermal management materials," ACS Appl. Mater. Interfaces 12(21), 24298–24307 (2020).
- 28. G. D. Zou, Z. W. Zhang, J. X. Guo, B. Z. Liu, Q. R. Zhang, C. Fernandez, and Q. M. Peng, "Synthesis of MXene/Ag composites for extraordinary long cycle lifetime lithium storage at high rates," ACS Appl. Mater. Interfaces 8(34), 22280-22286 (2016).
- 29. Z. W. Zhang, H. N. Li, G. D. Zou, C. Fernandez, B. Z. Liu, Q. R. Zhang, J. Hu, and Q. M. Peng, "Self-reduction synthesis of new MXene/Ag composites with unexpected electrocatalytic activity," ACS Sustainable Chem. Eng. **4**(12), 6763–6771 (2016).
- 30. E. Satheeshkumar, T. Makaryan, A. Melikyan, H. Minassian, Y. Gogotsi, and M. Yoshimura, "One-step solution processing of Ag, Au and Pd@MXene hybrids for SERS," Sci. Rep. 6(1), 32049 (2016).

#### 1409

## Optical Materials EXPRESS

- R. P. Pandey, K. Rasool, V. E. Madhavan, B. Aïssa, Y. Gogotsi, and K. A. Mahmoud, "Ultrahigh-flux and fouling-resistant membranes based on layered silver/MXene (Ti<sub>3</sub>C<sub>2</sub>T<sub>x</sub>) nanosheets," J. Mater. Chem. A 6(8), 3522–3533 (2018).
- 32. N. Li, Y. Jiang, Y. Xiao, B. Meng, C. Y. Xing, H. Zhang, and Z. C. Peng, "A fully inkjet-printed transparent humidity sensor based on a Ti<sub>3</sub>C<sub>2</sub>/Ag hybrid for touchless sensing of finger motion," Nanoscale **11**(44), 21522–21531 (2019).
- 33. B. S. Kalanoor, P. B. Bisht, S. A. Ali, T. T. Baby, and S. Ramaprabhu, "Optical nonlinearity of silver-decorated graphene," J. Opt. Soc. Am. B 29(4), 669–675 (2012).
- 34. Y. Yu, J. H. Si, L. H. Yan, M. Li, and X. Hou, "Enhanced nonlinear absorption and ultrafast carrier dynamics in graphene/gold nanoparticles nanocomposites," Carbon 148, 72–79 (2019).
- 35. M. M. Yue, J. H. Si, L. H. Yan, Y. Yu, and X. Hou, "Enhanced nonlinear optical properties of reduced graphene oxide decorated with silver nanoparticles," Opt. Mater. Express 8(3), 698–703 (2018).
- 36. Y. M. Xu, L. H. Yan, J. H. Si, M. Li, Y. Y. Ma, J. L. Li, and X. Hou, "Nonlinear absorption properties and carrier dynamics in MoS<sub>2</sub>/Graphene van der Waals heterostructures," Carbon 165, 421–427 (2020).
- 37. Y. B. Shao, C. Chen, J. Han, D. G. Kong, W. Z. Wu, and Y. C. Gao, "Wavelength-dependent nonlinear absorption and ultrafast dynamics process of WS2," OSA Continuum 2(9), 2755–2763 (2019).
- 38. J. Li, Z. L. Zhang, L. Du, L. L. Miao, J. Yi, B. Huang, Y. H. Zou, C. J. Zhao, and S. C. Wen, "Highly stable femtosecond pulse generation from a MXene Ti<sub>3</sub>C<sub>2</sub> fiber laser," Photonics Res. **7**(3), 260–264 (2019).
- Y. B. Shao, C. Chen, J. Han, D. G. Kong, W. Z. Wu, and Y. C. Gao, "Enhanced nonlinear optical absorption of WS<sub>2</sub> by Ag nanoparticles," Ferroelectrics 563(1), 177–186 (2020).
- V. Nguyen, J. H. Si, L. H. Yan, and X. Hou, "Direct demonstration of photoluminescence originated from surface functional groups in carbon nanodots," Carbon 108, 268–273 (2016).